A Method for the Reversible Trapping of Proteins in Non-Native Conformations[†]

Lilia Milanesi,[‡,§] Clare Jelinska,[‡] Christopher A. Hunter,*[,§] Andrea M. Hounslow,[‡] Rosemary A. Staniforth,[‡] and Jonathan P. Waltho*[,‡,||]

Department of Molecular Biology and Biotechnology, The University of Sheffield, Sheffield S10 2TN, U.K., Centre for Chemical Biology, Krebs Institute for Biomolecular Science, Department of Chemistry, The University of Sheffield, Sheffield S3 7HF, U.K., and Faculty of Life Sciences and Manchester Interdisciplinary Biocentre, The University of Manchester, Manchester M1 7DN, U.K.

Received July 21, 2008; Revised Manuscript Received October 19, 2008

ABSTRACT: High-dilution equilibrium macrocyclization is developed as a general approach to trapping proteins in a non-native state with a synthetic cross-linking agent. The approach is illustrated using the N-terminal domain of phosphoglycerate kinase and a synthetic reagent containing two maleimide groups, for selective attachment to cysteines introduced onto the protein surface through mutagenesis, and an aromatic disulfide that can be chemically or photochemically cleaved. Following functionalization of the cysteine residues, thiol−disulfide exchange chemistry under strongly unfolding conditions was used to achieve intramolecular cyclization and a high yield of the cross-linked protein. ^{1}H NMR, CD, and fluorescence spectroscopies indicate that the conformation of the cross-linked protein is non-native. Chemical cleavage of the aromatic disulfide cross-link by a reducing agent results in the acquisition of a nativelike conformation for the reduced protein. Thus, the cross-link acts as a reversible switch of protein folding.

The elucidation of the mechanism by which proteins acquire their three-dimensional structure is important for understanding their biological activity. The spontaneous refolding of many proteins in vitro indicates that the information needed to specify the native structure and biological activity of a protein is generally contained in its amino acid sequence (*1*). Experimental investigations and computational studies of folding reactions play a major role in deciphering the link between the structure and function of proteins (*2*−*5*) and have identified a wide range of partially folded forms of proteins present within the folding landscape. Examples include transiently populated, intermediate species populated during folding reactions, some of which appear to assist and some to retard progression from the denatured to the native state (*6*−*9*), and species that appear as a prelude to misfolding, including the assembly of insoluble aggregates that are characteristic of a range of debilitating diseases (*10*−*13*). For some proteins, conditions can also be found where long-lived partially folded states are populated measurably, and a wide range of so-called molten globule species have been characterized (*14*−*18*).

Relating partially folded forms to protein folding landscapes is, however, usually not straightforward. Under solution conditions favoring folding, the population of partially folded states is normally substantially disfavored, and destabilizing mutations or amino acid deletions are employed to generate irreversibly trapped species (*19, 20*). One exception where reversibility can be achieved is the study of proteins for which folding is coupled to the binding of specific ligands, a system that has been used successfully in biotechnology applications (*21, 22*). When not a property of the wild-type protein, amino acid deletions can sometimes be used to generate partially folded states that can recover to a nativelike state upon binding to a target ligand. Reversibility can also be achieved where partially folded species can be selectively stabilized under acidic or mild chemical denaturing conditions, but again this opportunity is not available for most proteins. A third way of achieving reversibility in the population of partially folded forms is to use the chemistry of thiol−disulfide exchange to isolate intermediate species and overcome their inherent instability (*23, 24*).

Photolabile disulfides linked to peptide fragments (*25, 26*) have been used to study submillisecond protein folding reactions that are not accessible using traditional stopped-flow mixing methods (*27*−*31*). In this approach, a photochemical group is introduced into a peptide by single-amino acid attachment or by linking of two side chains (cyclization) (*25, 26, 32*−*34*). The photochemical group constrains the peptide in a non-native conformation, and the native state can be recovered by selective optical excitation of the chromophore. However, these methods have been successfully applied only to peptides, because the chemistry is based on solid phase techniques, which cannot be easily applied to most proteins (*35*−*37*). Intramolecular cyclization, achieved via the introduction of disulfide cross-links and peptide and nonpeptide linkers, has also been used to study the effect

[†] This work was supported by BBRSC Grant BBS/B/10218 to C.A.H. and J.P.W. We thank the BBRSC, EPSRC, The Royal Society, and the White Rose Fellowship for financial support. R.A.S. is a Royal Society University Research Fellow.

* To whom correspondence should be addressed. E-mail: c.hunter@shef.ac.uk or j.waltho@shef.ac.uk.

[‡] Department of Molecular Biology and Biotechnology, The University of Sheffield.

[§] Department of Chemistry, The University of Sheffield.

[||] The University of Manchester.

10.1021/bi801362f CCC: $40.75
Published on Web 11/26/2008

of chain topology on the folding kinetics of two-state proteins (*38, 39*).

The studies above highlight the potential of intramolecular cyclization as an effective way of perturbing the native fold, if a more generally applicable methodology was available. If these species can be trapped reversibly, as in the disulfide cross-linked proteins, the cyclized proteins can be used to study fast folding reactions and the folding of metastable species that are not sufficiently populated under normally attainable conditions. Cyclization perturbs the free energy landscape available to the protein, which leads to distortions of the population distribution of accessible conformers compared with the non-cross-linked protein. Once the cyclization is broken, the landscape reverts to that of the non-cross-linked protein, whereby the starting distribution of conformers is determined by the effects of the cross-link. In some circumstances, the starting distribution may lead to folding trajectories that differ substantially from those taken by a protein that is folding following denaturation using pH, temperature, pressure, or chemical denaturant (depending on the rates of equilibration of the denatured states vs the rates of folding or misfolding), while in others, equilibration of the denatured state will precede the crossing of the major transition state barrier to refolding. Importantly, folding from an initially cyclized protein chain has an advantage in that the position of the initial cyclization can be varied, and hence, folding starting at widespread regions of the energy landscape of the non-cross-linked protein can be assessed.

Here we describe a method that can be applied widely to cyclize proteins reversibly, which we demonstrate using the selective attachment of a linker that cross-links two side chains of a 174-residue protein. The linker has the capacity for both chemical and photochemical cleavage. We show that the cyclized protein adopts a non-native conformational distribution and that chemical cleavage of the linker restores the folded state. Thus, the linker acts as a reversible switch between a partially folded state and the native state.

EXPERIMENTAL PROCEDURES

Materials and Methods. Chemicals and solvents were obtained from commercial sources and used without further purification. Buffer exchange and concentration of proteins were carried out using Vivaspin centrifugal devices (molecular mass cutoff of 10000 Da, polyethersulfone membrane, 20 mL capacity) purchased from Sartorious Vivascience. Prepacked G-25 PD10 columns were purchased from A. Pharmacia and used for buffer exchange and removal of compounds with molecular masses of <5000 Da from the protein solutions. Size exclusion chromatography (SEC)[1] was carried out using a Perkin-Elmer series 200 autosampler, an UV−vis diode array detector set at 280 nm, and a pump connected to a Shodex KW-803 column. All buffers contained 3 mM NaN_3 as a preservative, and for the reaction of the proteins with **1**, the solutions were degassed as previously described (*40*). ^1H and ^{13}C NMR spectra of **1** and the model disulfide were recorded on either Bruker AMX400 or AMX500 spectrometers. All chemical shifts are quoted in parts per million, and spectra were referenced indirectly using the solvent signal. Positive ESI-MS spectra were recorded on a Fison VG Platform using a quadrupole detection system. MALDI/MS spectra were obtained using a Micromass TOF Spec2E mass spectrometer. ESI-FTICR-MS spectra were obtained using a 9.4 T-Bruker Bioapex II spectrometer and an external electrospray ionization source (Analitica, Bradford, CT) (*41*).

Computational Methods. Molecular mechanics calculations were performed using the AMBER force field as implemented in Macromodel 4.0 (*42*). For this purpose, we used a simplified derivative of **1**, where two CH_3CH_2S fragments were attached to the maleimides as a model of the cysteines in the protein. A Monte Carlo conformational search was used to identify low-energy conformers. To model the cross-linked state, geometrical constraints were imposed according to the relative distance and angular orientation of the thiol side chains in the protein (CH_3-CH_3' distance of 27.65 Å; CH_2-CH_2' distance of 29.6 Å; $CH_3-CH_2-CH_2'$ angle of 115.9°; $CH_3'-CH_2'-CH_2$ angle of 145.8°; $CH_3-CH_2-CH_2'-CH_3'$ dihedral angle of 75.9°). The distances and angles used here are those of the side chain carbons of wild-type N-PGK (E108 and R118) and are taken from the X-ray crystal structure of PGK (*43*). The relative position of the cysteine side chains (C108 and C118) in the N-PGK mutant was assumed to be essentially the same. The calculations were performed for all diastereoisomers (*RR*, *SS*, and *RS*).

Preparation of wt N-PGK (wt-P) and the N-PGK Mutant (F17W/C18V/E108C/R118C) (m-P). Mutagenesis was carried out using the QuikChange method (Stratagene). Only single-amino acid substitutions were performed in any one reaction. Primers were supplied by MWG Biotech, and mutagenesis was confirmed by DNA sequencing performed within the Department of Molecular Biology and Biotechnology at The University of Sheffield. ***wt*-P** and the mutant ***m*-P** were expressed using pET5a expression vectors and purified according to previous protocols (*44*), with the exception that for ***m*-P**, all the buffers used contained 2 mM DTT. Both proteins were stored as suspensions in 80% (w/v) ammonium sulfate in 50 mM TRIS and 100 mM NaCl (pH 7.5) for ***wt*-P**, and the same buffer but also containing 4 mM DTT and 1 mM EDTA for ***m*-P**. The concentration of proteins was determined in buffers without DTT present using the absorbance at 280 nm ($\varepsilon_{280} = 10500\ M^{-1}\ cm^{-1}$ for ***m*-P** and $\varepsilon_{280} = 5000\ M^{-1}\ cm^{-1}$ for ***wt*-P**). CD and ^1H NMR were used to test the correct folding of each protein in the relevant buffer.

Recovery of Protein from 80% Ammonium Sulfate and Removal of DTT. For ***wt*-P**, an aliquot of suspension was centrifuged and the precipitated protein redissolved in the relevant buffer. The solution (0.4 mL) was exchanged three times in the relevant buffer (20 mL) using centrifugal devices and was used immediately for the reaction with **1**. For ***m*-P**, the precipitated protein recovered after centrifugation of the ammonium sulfate suspension was dissolved in fresh 50 mM

[1] Abbreviations: SEC, size exclusion chromatography; ESI-MS, electrospray ionization mass spectrometry; MALDI-MS, matrix-assisted laser desorption ionization mass spectrometry; ESI-FTICR-MS, electrospray ionization Fourier transform ion-cyclotron resonance mass spectrometry; AMBER, assisted model building with energy refinement; N-PGK, N-terminal domain of phosphoglycerate kinase from *Geobacillus stearothermophilus*; *wt*, wild type; DTT, dithiothreitol; TRIS, tris(hydroxymethyl)aminomethane; EDTA, ethylenediaminetetraacetic acid; CD, circular dichroism; NMR, nuclear magnetic resonance; DTNB, 5,5′-dithiobis(2-nitrobenzoic acid); GuHCl, guanidinium hydrochloride; NEM, *N*-ethylmaleimide; TSP, 3-(trimethylsilyl)propionate; NATA, *N*-acetyl-L-tryptophan amide.

TRIS, 10 mM DTT, and 1 mM EDTA (pH 8.0). The solution (100−200 μM protein) was left at room temperature for at least 6 h and then loaded on a PD10 column previously equilibrated with 20 mM potassium acetate (pH 5.0) to remove excess DTT. The protein (20−40 μM) eluted DTT free in the first 2 mL, as tested by size exclusion chromatography, and was used immediately for the reaction with **1** (***m*-P**, t_R = 11.2 min and oxidized DTT t_R = 15.2 min in a 20 mM potassium acetate (pH 5.0) eluent, with a flow rate of 1 mL/min). The amount of free thiol was also determined using a standard DTNB assay (ε_{412}TNB = 14150 M^{-1} cm^{-1}) (*45, 46*).

*Preparation of wt N-PGK Functionalized with **1**) (**fwt-P**).* To a 5 mL vial equipped with a magnetic stirrer were added the following in order: 800 μL of 6 M GuHCl in 50 mM sodium phosphate (pH 6.5), 750 μL of 50 mM sodium phosphate (pH 6.5), 800 μL of CH_3CN, 10 μL of 2.5 mM **1** in CH_3CN, and 40 μL of 360 μM ***wt*-P** in 50 mM sodium phosphate (pH 6.5). The solution was left stirring for 12 h at room temperature under nitrogen, and then it was transferred into a centrifugal device and buffer exchanged with water. An aliquot (20−40 μL) of the resulting 500 μL solution was added to a solution of 10 mg/mL sinapinic acid (3,5-dimethoxy-4-hydroxycinnamic acid) in acetone (50%, v/v), dried under nitrogen, and subjected to MALDI-MS. As a control, a sample of pure ***wt*-P** was prepared for mass spectrometry analysis as follows. Ten microliters of 0.32 mM ***wt*-P** in 50 mM sodium phosphate (pH 6.5) was diluted to 20 mL with water in a centrifugal filter device, and the sample was concentrated. An aliquot of the resulting sample (500 μL, 50 μM) was mixed with a 1:1 mixture of CH_3CN and 2% formic acid (50%, v/v) and subjected to ESI-MS. Expected for ***fwt*-P** (amino acids 1−174, $C_{873}H_{1393}N_{248}O_{257}S_6$): *m/z* 19666. Found: *m/z* 19690 [$(M + Na)^+$]. Expected for ***wt*-P** (amino acids 1−174, $C_{853}H_{1380}N_{246}O_{253}S_4$): *m/z* 19258. Found: *m/z* 19260 [$(M + H)^+$].

*Preparation of Reduced wt N-PGK Functionalized with **1** (**fwt-P$_{red}$**).* A solution of ***fwt*-P** (2.4 mL) was transferred to a centrifugal filter device and diluted to 20 mL with a fresh solution of 1 mM DDT in 2 M GuHCl and 50 mM sodium phosphate (pH 7.0). The solution volume was reduced by centrifugation to 500 μL and the solution transferred to a 2 mL Eppendorf vial equipped with a magnetic stirrer. After 12 h, the reaction mixture was transferred into a centrifugal filter device and the buffer exchanged with water. An aliquot of the resulting sample (500 μL) was treated as described for mass spectrometry analysis of ***wt*-P** and then subjected to ESI-MS. Expected for ***fwt*-P$_{red}$** ($C_{863}H_{1387}N_{247}O_{255}S_5$): *m/z* 19463. Found: *m/z* 19464 [$(M + H)^+$].

*Preparation of Functionalized N-PGK Dimer (**fwt-P$_{ox}$**).* The procedure describing the preparation of ***fwt*-P** was scaled up to give 18 mL of reaction mixture containing 6 μM ***wt*-P**. The solution was treated as described for the preparation of ***fwt*-P$_{red}$** to give 0.5−1.0 mL of ***fwt*-P$_{red}$** (∼200−400 μM) in 1 mM DTT, 2 M GuHCl, and 50 mM sodium phosphate (pH 7.0). Removal of DTT was carried out as follows. The solution was loaded in a centrifugal device, diluted 20−40-fold in 2 M GuHCl and 50 mM sodium phosphate (pH 7.0), and concentrated 20−40-fold. This procedure was repeated three times, and the resulting solution (0.5−1.0 mL, ∼200−400 μM ***fwt*-P$_{red}$**) was left for 12 h under gentle stirring in an open vial. Samples for mass spectrometry (ESI) were prepared as follows: 0.5−1.0 mL of the reaction mixture was loaded on a Sephadex G-25 column (PD10, Pharmacia) and eluted with water. An aliquot of the first 2.5 mL of eluate was treated as described for ***fwt*-P$_{red}$** and submitted to ESI-MS. Expected for ***fwt*-P$_{ox}$** ($C_{1726}H_{2770}N_{494}O_{510}S_{10}$): *m/z* 38926. Found: *m/z* 38962 [$(M + 2H_2O)^+$], *m/z* 19480 [$(M + 2H_2O)^{2+}$].

*Preparation of Functionalized Mutant N-PGK under Unfolding Conditions (**fm-P**).* To a 5 mL vial equipped with a magnetic stirrer were added the following in order: 800 μL of 6 M GuHCl in 50 mM sodium phosphate (pH 6.5), 750 μL of 50 mM sodium phosphate (pH 6.5), 800 μL of CH_3CN, 10 μL of 2.5 mM **1** in CH_3CN, and 600 μL of 24−40 μM ***m*-P** in 20 mM CH_3COOK (pH 5.0). The final pH of the reaction mixture was 6.5, and the solution was left stirring for 12 h at room temperature under nitrogen. It was then transferred into a centrifugal device, diluted with water to 20 mL, and concentrated to 1−2 mL. This procedure was repeated three times to remove the denaturant and the excess of **1**. An aliquot (20−40 μL) of the concentrated solution was mixed with a 1:1 mixture of CH_3CN and 2% formic acid (50%, v/v) and subjected to ESI-FTICR-MS. As a control, a sample of DTT free ***m*-P** was prepared for mass spectrometry analysis: removal of DTT was carried as described in the previous section except that a 0.1% (v/v) acetic acid solution was used as the eluent. An aliquot of 20−40 μL was mixed 1:1 with a solution of sinapinic acid as described above, dried under a stream of nitrogen, and subjected to MALDI-MS. Expected for ***m*-P** (amino acids 1−174, $C_{852}H_{1376}N_{244}O_{251}S_5$): *m/z* 19214. Found: *m/z* 19214 (M^+), *m/z* 19085 [M − N-terminal methionine$)^+$], *m/z* 9607 [$(M/2)^+$]. Expected for ***fm*-P** ($C_{892}H_{1403}N_{248}O_{259}S_9$): *m/z* 20030. Found: *m/z* 19622 [$(M)^+$ for ***fm*-P$_{ox}$**], *m/z* 19645 [$(M + Na)^+$ for ***fm*-P$_{ox}$**], *m/z* 19668 [$(M + 2Na)^+$ for ***fm*-P$_{ox}$**], *m/z* 19691 [$(M + 3Na)^+$ for ***fm*-P$_{ox}$**], *m/z* 19714 [$(M + 4Na)^+$ for ***fm*-P$_{ox}$**], *m/z* 19491 [$(M$ − methionine$)^+$ for ***fm*-P$_{ox}$**], *m/z* 19514 [$(M + Na$ − methionine$)^+$ for ***fm*-P$_{ox}$**], *m/z* 19418 [$(M - 204)^+$ for ***fm*-P$_{ox}$**], *m/z* 19441 [$(M + Na - 204)^+$ for ***fm*-P$_{ox}$**], *m/z* 19826 [$(M + 204)^+$ for ***fm*-P$_{ox}$**], *m/z* 19849 [$(M + 204 + Na)^+$ for ***fm*-P$_{ox}$**].

*Reaction of DTT and NEM with the Reaction Mixture of **fm-P**.* The reaction mixture of ***fm*-P** and **1**, prepared as described above, was transferred to a centrifugal filter device and diluted to 20 mL with a fresh solution of 1 mM DTT, 2 M GuHCl, and 50 mM sodium phosphate (pH 7.0). Centrifugal buffer exchange was carried out as described for ***fwt*-P$_{red}$**, and it was used to remove excess **1** and change the composition of the reaction mixture for the reduction of the aromatic disulfide. The solution was centrifuged to a final volume of 500−700 μL, then transferred to a 1 mL Eppendorf vial equipped with a magnetic stirrer, and incubated for 12 h to ensure completion of the reduction reaction. The solution was then transferred into a centrifugal filter device and diluted to 20 mL with a fresh solution of 2 mM NEM and 2 M GuHCl in 50 mM sodium phosphate (pH 6.5). The volume was reduced by centrifugation to 500 μL and the resulting sample transferred into a 2 mL Eppendorf vial equipped with a magnetic stirrer. After being stirred for 4 h, reaction mixture was transferred in a centrifugal filter device and the buffer exchanged with water. An aliquot of the resulting sample (500 μL) was used to

prepare a sample for ESI-FTICR-MS as described above for ***fm*-P**. Expected for DTT/NEM labeling of ***fm*-P_{ox}** in the reaction mixture of ***fm*-P** ($C_{884}H_{1406}N_{248}O_{259}S_7$): *m/z* 19874. Found: *m/z* 19874 (M^+), *m/z* 19897 [$(M + Na)^+$], *m/z* 19990 [$(M + 2Na)^+$], *m/z* 19669 [$(M - 204)^+$], *m/z* 19692 [$(M + 2Na)^+$], *m/z* 19715 [$(M + 2Na)^+$], *m/z* 19743 [(M − methionine)$^+$].

*Preparation of the Functionalized N-PGK Mutant under Native Conditions (**fm*-P_{ox}*).* This procedure was identical to the preparation under unfolding conditions described above with the exception that denaturant was omitted in the first step of the reaction. The procedure was also scaled up. To 12.4 mL of a 6 μM ***m*-P** reaction mixture in a 50 mL flask were added the following in order: 8 mL of 50 mM sodium phosphate (pH 6.5), 2.6 mL of CH_3CN, 0.4 mL of 2.5 mM **1** in CH_3CN, and 1.4 mL of 47 μM ***m*-P** in 20 mM potassium acetate (pH 5.0). The reaction mixture was left stirring for 12 h under nitrogen. The solution was transparent for the first 3 h and then showed a precipitate. The reaction was quenched and the precipitate completely dissolved by dilution with a solution of 5 mM DTT, 2 M GuHCl, and sodium phosphate (pH 7.0) (unfolding buffer). Aliquots of the reaction mixture (2 mL) were loaded into a centrifugal device, diluted to 20 mL with unfolding buffer, and then concentrated to 1−2 mL. This procedure was repeated three times to remove unreacted **1**. The resulting solution (1.4 mL, ~60 μM) was transferred to an Eppendorf vial and left stirring for 12 h. Removal of DTT was carried out under unfolding conditions as follows: 1.4 mL of the reaction mixture was diluted to 20 mL with 2 M GuHCl and 50 mM sodium phosphate (pH 7.0) and concentrated to 2−4 mL. This procedure was repeated four times to give a 4 mL (~18 μM) solution, free of DTT. This solution was left stirring for 12 h in an open vial. To remove GuHCl, the solution was loaded onto a Sephadex G-25 desalting column (PD10, Pharmacia) equilibrated with water (for samples subjected to mass spectrometry) or 50 mM sodium phosphate and 100 mM NaCl (pH 7.0) (for samples analyzed using CD, fluorescence, and ^{1}H NMR). The GuHCl-free protein was collected in the first 2 mL of eluate, as tested by size exclusion chromatography [***fm*-P_{ox}**, t_R = 11.2 min and GuHCl t_R = 13−14 min in 50 mM sodium phosphate and 100 mM NaCl (pH 7.0) as the eluent with a flow rate of 1 mL/min]. For ESI-MS, the same procedure described for the preparation of ***fm*-P** under unfolding conditions was used. The yield of the reaction was 30−40%, as estimated by UV−vis absorbance using an ε_{280} of 42401 M^{-1} cm^{-1}. This was calculated using the ε_{280} of the model disulfide and that of ***m*-P** [$\varepsilon_{(fm\text{-}Pox)280} = \varepsilon_{(m\text{-}P)280} + \varepsilon_{(model\ disulfide)280}$]. Expected for ***fm*-$P_{ox}$** ($C_{872}H_{1390}N_{246}O_{255}S_7$): *m/z* 19622. Found: *m/z* 19622 (M^+), *m/z* 19643 [$(M + H_2O)^+$], *m/z* 19662 [$(M + 2H_2O)^+$], *m/z* 19690 [$(M + 3H_2O)^+$], *m/z* 19491 [(M − methionine)$^+$], *m/z* 19512 {[(M − methionine) + H_2O]$^+$}, *m/z* 19530 {[(M − methionine) + $2H_2O$]$^+$}, *m/z* 19546 {[(M − methionine) + $3H_2O$]$^+$}.

*Reaction of DTT and NEM with **fm*-P_{ox}*.* ***fm*-P_{ox}** (400 μL, ~60 μM) in water was used to prepare four samples (100 μL each) for mass spectrometry. One sample was analyzed as described for ***fm*-P_{ox}**, and the ESI-MS results are reported above. NEM (1 mM) was added to another sample and incubated for 2 h prior to ESI-MS. The mass spectrum of the NEM-treated ***fm*-P_{ox}** sample was identical to that of ***fm*-P_{ox}** as reported above. DTT (0.3 mM) was added to the remaining two samples, and each was incubated at room temperature for 4 h. One of these two sample was analyzed by ESI-MS as described for ***fm*-P_{ox}**, and 1 mM NEM was added to the other sample, incubated for 2 h at room temperature, and then subjected to ESI-MS. Expected for ***fm*-P_{red}** (***fm*-P_{ox}** with DTT) ($C_{872}H_{1392}N_{246}O_{255}S_7$): *m/z* 19624. Found: *m/z* 19624 (M^+), *m/z* 19645 [$(M + H_2O)^+$], *m/z* 19664 [$(M + 2H_2O)^+$], *m/z* 19692 [$(M + 3H_2O)^+$], *m/z* 19493 [(M − methionine)$^+$], *m/z* 19514 {[(M − methionine) + H_2O]$^+$}, *m/z* 19532 {[(M − methionine) + $2H_2O$]$^+$}, *m/z* 19548 {[(M − methionine) + $3H_2O$]$^+$}. Expected for ***fm*-P_{ox}** with DTT and NEM ($C_{884}H_{1406}N_{248}O_{259}S_7$): *m/z* 19874. Found: *m/z* 19877 (M^+), *m/z* 19897 [$(M + H_2O)^+$], *m/z* 19990 [$(M + 2H_2O)^+$], *m/z* 19747 [(M + H − methionine)$^+$], *m/z* 19765 {[(M − methionine) + H_2O]$^+$}.

*Preparation of Mutant N-PGK Labeled with NEM (**m*-P_{nem}*).* ***m*-P_{nem}** was prepared following the same procedure described for the preparation of ***fm*-P_{ox}** under native conditions, except that 50 μL of 48 mM NEM in 50 mM sodium phosphate (pH 6.5) were added to the reaction mixture (12.4 mL) in place of disulfide **1**. The reaction mixture was stirred gently under nitrogen for 12 h. It was diluted to 24 mL with 2 M GuHCl and 50 mM sodium phosphate (pH 6.5) and concentrated to ~2 mL in a centrifugal device. GuHCl and excess NEM were removed by loading the 2 mL sample on a PD10 column equilibrated in 50 mM sodium phosphate and 100 mM NaCl (pH 7.0). ***m*-P_{nem}** eluted in the fractions corresponding to the first 2.5 mL. The yield of the reaction was 97%, as calculated by UV−vis absorbance using the extinction coefficient of ***m*-P** (ε_{280} = 10500 cm^{-1} M^{-1}) for ***m*-P_{nem}**.

*Preparation of a Model Disulfide Composed of Two N-Acetylcysteines Attached to **1**.* The procedure for the preparation of this compound has been reported previously (*40*). ^{1}H NMR (400 MHz, DMSO-d_6): δ 12.96 (broad, 2H), 8.39 (d, J = 8.0 Hz, 2H), 8.38 (d, J = 8.12 Hz, 2H), 7.71 (d, J = 8.60 Hz, 4H), 7.36 (m, 4H), 4.50 (m, 2H), 4.20 (m, 2H), 3.35 (m, 2H), 3.20 (dd, J = 5.40, 13.40 Hz, 1H), 3.08 (dd, J = 8.16, 13.44 Hz, 1H), 2.90 (m, 1H), 1.90 (s, 3H), 1.89 (s, 3H). ^{13}C NMR (500 MHz, DMSO-d_6): δ 176.14, 176.03, 174.43, 174.40, 172.35, 172.30, 169.86, 169.75, 136.19, 131.95, 128.42, 128.40, 127.81, 66.77, 52.38, 51.91, 36.61, 36.37, 33.13, 32.96, 22.78. HRMS (ES^+): expected for $C_{28}H_{30}N_4O_8S_4$ $(M + H)^+$ *m/z* 735.0923, found *m/z* 735.0919. UV−vis [50 mM sodium phosphate and 100 mM NaCl (pH 7.0)]: ε_{250} = 34883 M^{-1} cm^{-1}, ε_{280} = 31901 M^{-1} cm^{-1}.

Protein NMR Measurements. One-dimensional NMR spectra of the proteins were recorded using a Bruker DRX600 spectrometer equipped with a cryoprobe. All spectra were internally referenced to TSP at 0.0 ppm. Spectra were recorded using a protein concentration of 80−100 μM at 25 °C in 50 mM sodium phosphate, 100 mM NaCl (pH 7.0), and 10% D_2O, or in the same buffer with GuHCl added to a final concentration of 1 M. DTT was added to the relevant samples to a final concentration of 1 mM. Spectra were recorded with 128 scans, and water suppression was achieved using a presaturation pulse during the relaxation delay between scans.

Circular Dichroism Measurements. Stock proteins solutions (60 μM) prepared in 50 mM sodium phosphate and

100 mM NaCl (pH 7.0) were diluted to 20 μM for CD measurements in the same buffer or in aliquots of a stock solution of 8 M urea prepared in the same buffer. DTT was added to these samples to give a concentration of 1 mM. Samples were allowed to denature for 4 h at 25 °C prior to DTT addition and recording of the spectra. The spectra of the blanks (denaturant in buffer) were also recorded. Samples of the model disulfide (20 μM) were prepared as described for the proteins. All CD spectra were recorded between 200 and 280 nm in a 1 mm path length cell using a scanning speed of 50 nm/min with a response time of 8 s. The spectra were averaged over two scans at 0.1 nm resolution and a bandwidth of 2 nm. The observed ellipticity (θ, millidegrees) was divided by $10Cl$ to convert to molar ellipticity [θ], where C is the concentration (moles per liter) and l the cell path length (centimeters).

Fluorescence Measurements. (i) Equilibrium Folding Measurements. Protein stock solutions (20 μM) were prepared in 50 mM sodium phosphate and 100 mM NaCl (pH 7.0). DTT at 10 mM was added to the stock solution of ***m*-P** and to half of the stock solution of ***fm*-$\mathbf{P_{ox}}$** (to give ***fm*-$\mathbf{P_{red}}$** in situ). The samples supplemented with DTT were kept at room temperature for 12 h before measurements. Samples for fluorescence measurements were prepared by dilution of the stock protein solutions in 50 mM sodium phosphate and 100 mM NaCl (pH 7.0) and aliquots of a stock solution of 6 M GuHCl prepared in the same buffer. The resulting samples (2 μM protein, 0−4 M GuHCl, and 1 mM DTT for ***m*-P** and ***fm*-$\mathbf{P_{red}}$**) were allowed to denature for 4 h at 25 °C before the spectra were recorded. The emission of the blank (denaturant in buffer) was also recorded. Emission spectra were recorded between 310 and 500 nm using an emission monochromator (slit width of 10 nm) and an excitation wavelength of 295 nm selected by a single monochromator (slit width of 2.5 nm) from the xenon light source of a Hitachi F-4500 fluorimeter. The reversibility of the unfolding reactions was established by diluting the unfolded samples with 1.8−4.0 μM protein in buffer without GuHCl. These samples, allowed to re-equilibrate for 4 h at the lower GuHCl concentrations, showed a fluorescence emission identical to that of corresponding samples which had reached equilibrium from the folded state. The data from the equilibrium unfolding measurements were fitted as a plot of the observed signal versus denaturant activity using an equation that describes a two-state model and takes into account the observed slopes in the pretransitional baselines (*47, 48*). Denaturant concentrations were converted to activity using a constant of 7.5 for $C_{0.5}$ (*47*). The observed signal used to calculate the denaturant dependence was the emission at 330 nm for ***m*-$\mathbf{P_{nem}}$** and ***m*-P** and at 345 nm for ***fm*-$\mathbf{P_{ox}}$** and ***fm*-$\mathbf{P_{red}}$**. Data were analyzed and fit using Microcal Origin 5.0, and the reported errors are those produced by the fitting algorithm within Origin.

(ii) Control Experiments. Stock solutions of NATA (500 μM) and model disulfide (1 mM) were prepared in 50 mM sodium phosphate and 100 mM NaCl (pH 7.0). Samples for fluorescence emission (2.8 μM) were prepared by dilution of these stock solutions in the same buffer with and without 1 mM DTT. Emission spectra were recorded in the same wavelength range and with the same instrumental setup described for the proteins (see Figure 3 of the Supporting Information). The effect of DTT quenching on the emission of the tryptophan in the native state was assessed by recording the emission of ***m*-$\mathbf{P_{nem}}$** in 50 mM sodium phosphate and 100 mM NaCl (pH 7.0) and in the same buffer with DTT added to a final concentration of 1 mM (see Figure 3 of the Supporting Information).

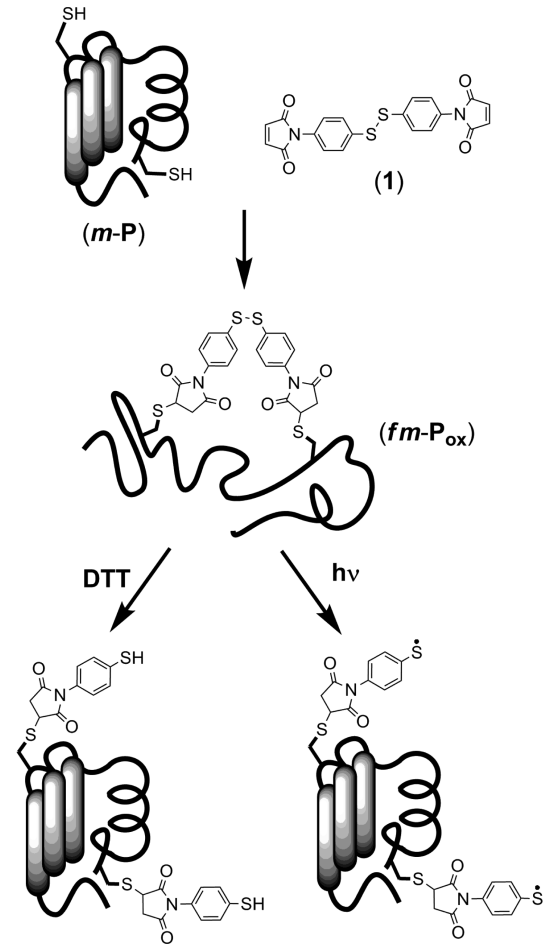

FIGURE 1: Strategy used to functionalize a protein with an aromatic disulfide cross-link (***fm*-$\mathbf{P_{ox}}$**). The protein (***m*-P**) contains exposed thiol groups for the reaction with the bismaleimide reagent (**1**). The aromatic disulfide acts as a constraint to force the protein into a non-native state (***fm*-$\mathbf{P_{ox}}$**). Reductive cleavage of the aromatic disulfide by addition of a reducing agent or by photolysis can be used to trigger the transition to a nativelike conformation.

RESULTS AND DISCUSSION

The approach to the preparation of a protein functionalized with a cleavable trigger (***fm*-$\mathbf{P_{ox}}$**) is shown in Figure 1: the bismaleimide derivative (**1**) incorporates an aromatic disulfide as the cleavable group and two maleimides for selective cross-linking of two cysteine residues engineered onto the surface of the protein of choice (***m*-P**). In this way, the trigger is part of an intramolecular cross-link that will maintain the cyclic protein in a non-native conformation, until it is released by chemical exposure or laser irradiation. The aromatic disulfide can be cleaved chemically by addition of a reducing agent, such as DTT, and this provides a convenient test that removal of the cross-link constraint promotes transition to a nativelike conformation. Reductive cleavage is one example of a range of nucleophilic cleavage reactions that can provide ways of triggering the refolding reaction. While the kinetics of reductive cleavage of cysteine disulfide bonds are relatively slow at millimolar concentra-

tions of DTT, this rate increases considerably for more activated and strained disulfide bonds (*24, 49*). Additionally, the presence of catalysts, such as selenol in addition to DTT, induces an increase of approximately 100-fold in the rate of native disulfide cleavage (*50*). Thus, without further modification of this first generation of linkers, potential triggering rates in excess of those of conventional mixing experiments should be achievable.

The selection of the chemistry underpinning the use of **1** as the cross-linking reagent is based on the following considerations. Maleimides are selective reagents for protein thiols (*51, 52*); while cysteine in its reduced state is relatively rare in proteins, it is tolerated in most parts of a protein fold, and it is readily incorporated using site-directed mutagenesis. Aromatic disulfide bonds are more susceptible to nucleophilic cleavage than their cysteine counterparts, and we and others have previously shown that they are readily cleaved in high yield on a picosecond time scale using laser photolysis (*26, 40*). Indeed, comparable linkers have been used as optical triggers for the study of peptide dynamics on the nanosecond time scale (*25, 26, 53, 54*) and for the recovery of enzyme activity on the microsecond time scale (*55*). We have also demonstrated previously the feasibility of the functionalization chemistry through the preparation of cysteine derivatives of **1** in water (*40*). Here we demonstrate procedures for translating the cross-linking methodology to intact proteins and establish that cross-linking does interfere with the native state in a reversible manner.

The N-terminal domain of phosphoglycerate kinase from *Geobacillus stearothermophilus* (N-PGK) was chosen to test the validity of the approach, since this protein has well-established folding properties, including the substantial population of a kinetic folding intermediate that acquires much of the native state organization in the millisecond or faster phase of the refolding reaction (*56, 57*). N-PGK comprises 174 residues and, therefore, is outside of the scope where solid phase synthesis of a cross-linked variant is readily achievable. Wild type N-PGK (***wt*-P**) contains a single cysteine residue, and thus, cross-linking with **1** would lead to an intermolecularly linked product. Hence, to establish methodology appropriate for intramolecular cross-linking, a mutant of N-PGK (***m*-P**) containing two cysteine residues was prepared. The structure of ***wt*-P** and the amino acids subjected to mutation are shown in Figure 2: the native cysteine at position 18, which is part of the hydrophobic core of N-PGK, was mutated to valine (C18V), and two surface residues (positions 108 and 118) were mutated to cysteine (E108C and R118C). In addition, a phenylalanine residue at position 17 was mutated to tryptophan (F17W) to provide a more intense fluorescence probe of folding. The far-UV CD and ^{1}H NMR spectra of variants bearing one or a combination of the mutations present in ***m*-P** (F17W and C18V) were not significantly different from those of the wild-type protein (***wt*-P**), indicating that the mutations do not perturb significantly the structure of the folded state. Equilibrium unfolding measurements (see below) indicated that the folded state of ***m*-P** has thermodynamic stability similar to that of native ***wt*-P**.

The choice of positioning of the two introduced cysteine residues was based on the crystal structure of full-length PGK, the NMR data for ***wt*-P**, and the chemistry required for the preparation of the cross-linked cyclic protein (*43, 57*).

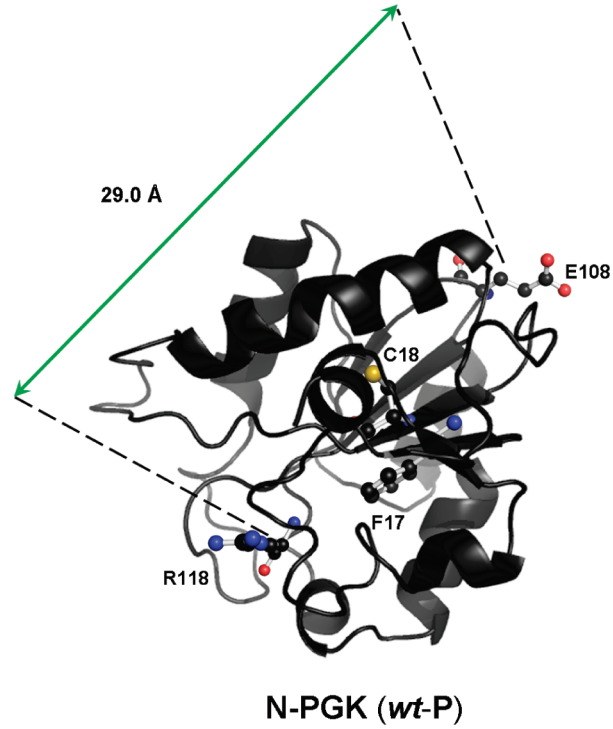

FIGURE 2: Three-dimensional structure of wild-type N-PGK (***wt*-P**) illustrated using PYMOL and taken from the three-dimensional structure of PGK from *G. stearothermophilus* (*43*). The amino acids subjected to mutation are highlighted. The native cysteine at position 18 was mutated to a valine (C18V) and the phenylalanine at position 17 to tryptophan (F17W), and the glutamate at position 108 and arginine at position 118 were mutated to cysteines (E108C and R118C, respectively). The distance in the native conformation between the β-carbons of the amino acids at positions 108 and 118 is shown.

Residues 108 and 118 are in loop regions of the native protein structure and are not involved in extensive surface interactions or in secondary structure elements. The residues are on opposite surfaces of the folded protein, where their β-carbons are separated by 29 Å, but are spaced only 10 amino acids apart in primary sequence and, thus, should have a relatively high effective molarity in the unfolded state. A Monte Carlo conformational search, using the AMBER force field in water (as implemented in Macromodel), showed that the distance between two amino acids attached to the maleimides of **1** is 6−13 Å for the low-energy conformers (*42*). If the cross-linker is constrained to span the 29 Å required to bridge the cysteines on the surface of the folded protein, the strain energy is estimated to be 250 kJ/mol (see Experimental Procedures for details). In addition, to accommodate the cross-linkage in the folded state, part of the cross-linker would necessarily interfere with the hydrophobic core arrangement of the native protein.

Synthesis of Intermolecularly Cross-Linked Protein. Initially, the preparation of an intermolecularly cross-linked species, using ***wt*-P** as the substrate (Scheme 1), was investigated to establish general conditions for the reaction of cysteine residues with **1**. Since ***wt*-P** contains only a single cysteine residue, the expected product was a protein dimer. The thiol of the protein was derivatized with **1** under unfolding conditions (2 M GuHCl) to release the single thiol of ***wt*-P** from the hydrophobic core. The formation of intermolecular disulfide dimers of unfolded ***wt*-P** was suppressed by working at a high protein dilution (6 μM) and

Scheme 1: Procedure Used for the Preparation of a ***wt*-P** Dimer Linked Using the Aromatic Disulfide Cross-Link (***fwt*-P_{ox}**) [a]

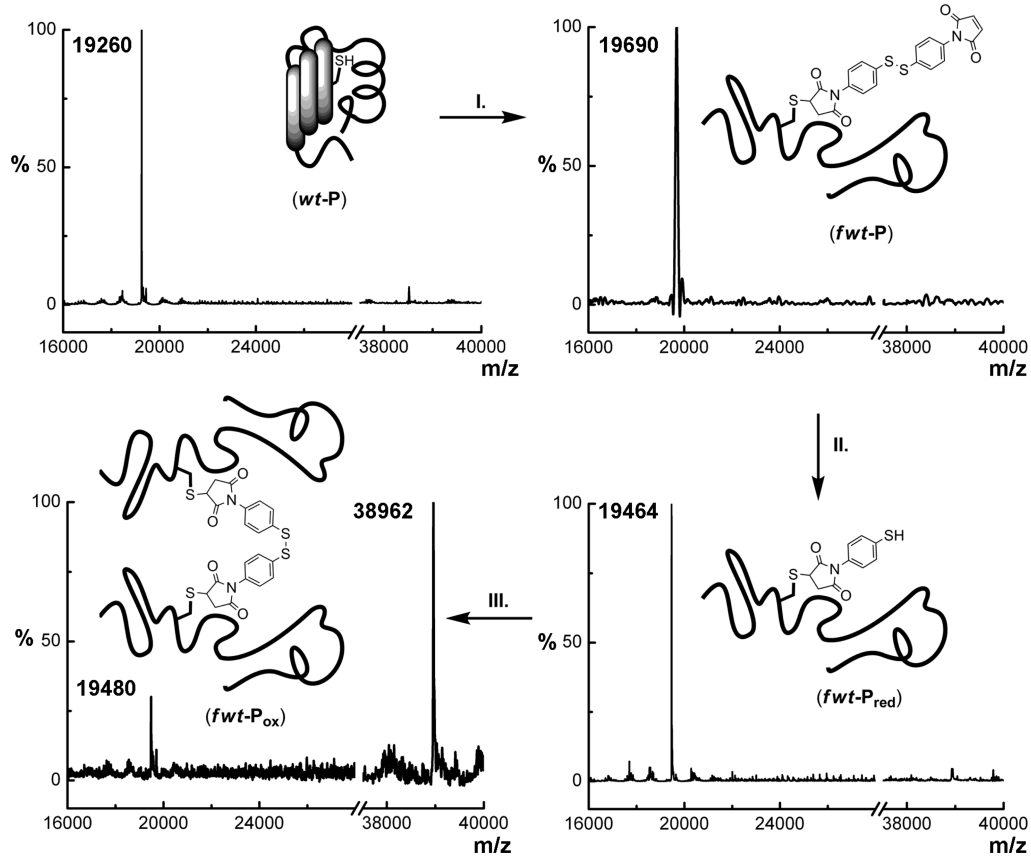

[a] The ESI or MALDI mass spectra of the products obtained from each step of the procedure are shown. Conditions: (i) 100 μM **1**, 50 mM sodium phosphate (pH 6.5), 3 mM NaN_3, 30% CH_3CN, 2 M GuHCl; (ii) 50 mM sodium phosphate (pH 7.0), 3 mM NaN_3, 1 mM DTT, 2 M GuHCl; (iii) 50 mM sodium phosphate (pH 7.0), 3 mM NaN_3, 100 mM NaCl.

maintaining a 20-fold excess of **1** over ***wt*-P**. To maintain such an excess of **1**, it was necessary to add 30% (v/v) acetonitrile to the reaction mixture. The reaction mixture was buffered at pH 6.5 to favor protonation of lysine, arginine, and histidine side chains and, thus, suppress their reaction with the maleimide groups of **1** (*52*). The functionalized protein intermediate (***fwt*-P**) was then treated with DTT, to cleave the aromatic disulfide. The resulting functionalized reduced protein (***fwt*-P_{red}**) was oxidized to afford a protein dimer linked by the aromatic cross-linker (***fwt*-P_{ox}**). The protein products were analyzed using mass spectrometry after removal of denaturant and excess **1** by centrifugal dialysis or size exclusion chromatography. The mass spectra were in agreement with expectation for each step of the procedure and are shown in Scheme 1. This indicates that under these experimental conditions the reaction of **1** with ***wt*-P** is selective, giving essentially quantitative yields of the desired products.

Synthesis of Intramolecularly Cross-Linked Protein. To translate the procedures described above to the preparation of an intramolecularly cross-linked species, the reaction of ***m*-P** with **1** was investigated (as described in Scheme 2). As ***m*-P** contains two cysteine residues, the production of a monomeric, cross-linked species is in competition with the formation of dimers and oligomers. The products of the reaction of ***m*-P** with **1** were again analyzed using mass spectrometry (Figure 3A). Four different protein species could be observed, none of which corresponded to the expected product, ***m*-P** functionalized with two molecules of **1**. No unreacted ***m*-P** was detected. The major product appeared at *m*/*z* 19622, which corresponds to the molecular weight of the final target, ***m*-P** functionalized with **1** as an intramolecular cross-link (***fm*-P_{ox}** in Scheme 2). The minor peak at *m*/*z* 19491 corresponds to the mass expected for ***fm*-P_{ox}**, which has lost a methionine from the N-terminal sequence. Loss of the same methionine was also observed for unreacted ***m*-P** and is a consequence of the expression system used for the preparation of the mutant protein. The two other peaks, at *m*/*z* 19418 and 19826, differ from the mass of ***fm*-P_{ox}** by $\pm$204, which corresponds to half the mass of the maleimide reagent (**1**). This pattern suggests that there are competitive reaction pathways involving thiol−disulfide exchange of the cysteines with the aromatic disulfide.

The experiments with ***wt*-P** indicate that reaction of the first cysteine with **1** should be a clean quantitative process to form intermediate **IP** in Scheme 2. This intermediate has four possible reaction pathways. The intermolecular reaction with **1** to give the desired product is not observed, so the three intramolecular processes shown in Scheme 2 dominate, presumably because of the high effective molarity for these reactions. The second cysteine thiol in intermediate **IP** can attack the cross-linking agent at the second maleimide, or at either of the disulfide sulfur atoms, to generate three different products that would account for the observed complexity in the mass spectrum (Scheme 2 and Figure 3A). The identities of these three products were confirmed by subjecting the

Scheme 2: Procedure Used for the Reaction of Protein ***m*-P** with **1** under Unfolding Conditions[a]

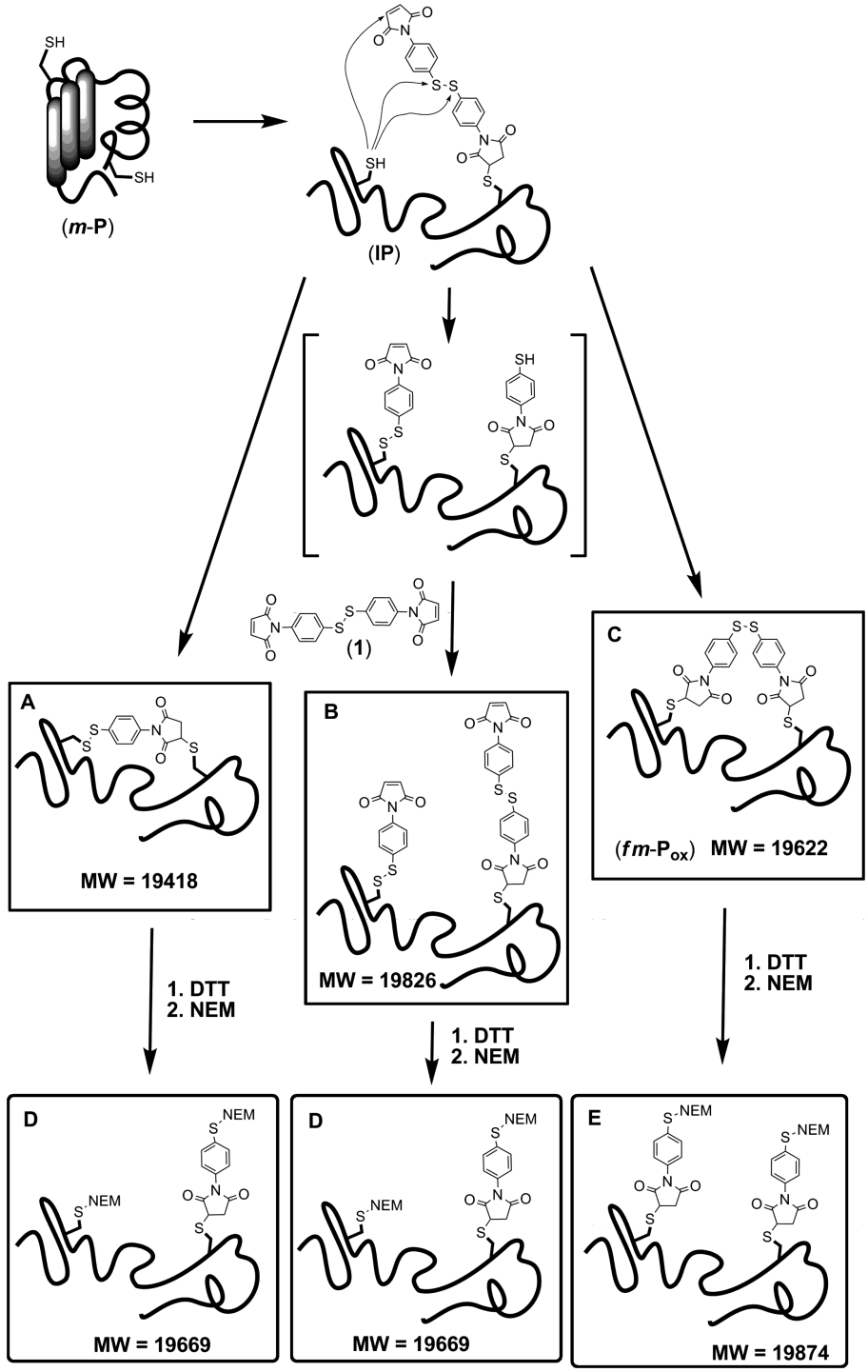

[a] The structure of intermediate **IP** is shown along with the three intramolecular processes that result in the three products (A, B, and C) observed in the mass spectrum shown in Figure 3A. Products D and E were observed after sequential addition of DTT and NEM to the reaction mixture. Conditions: (i) 100 μM **1**, 50 mM sodium phosphate (pH 6.5), 3 mM NaN_3, 30% CH_3CN, 2 M GuHCl.

crude reaction mixture to DTT to reduce all of the disulfides and then addition of *N*-ethylmaleimide (NEM) to label all exposed thiols (Scheme 2). The mass spectrum of the DTT/NEM products showed only three protein signals consistent with the analysis given above (Figure 3). The peak at *m*/*z* 19874 corresponds to the peak at *m*/*z* 19622 in the starting material plus two NEM groups, and this pattern confirms that the fragment at *m*/*z* 19622 corresponds to the intramolecularly cross-linked mutant ***fm*-P$_{ox}$**. The peak at *m*/*z* 19743 corresponds to the peak at *m*/*z* 19491 in the starting material plus two NEM groups, and this confirms the presence of the N-methionine-truncated ***fm*-P$_{ox}$** in the reaction mixture. The peak at *m*/*z* 19699 corresponds to the peak at *m*/*z* 19418 in the starting material plus two NEM groups, as well as to the peak at *m*/*z* 19826 in the starting material, which has lost the mass of half of **1** (MW = 204) and added two NEM groups. This coincidence is the source of the simplification of the mass spectrum of the NEM adducts.

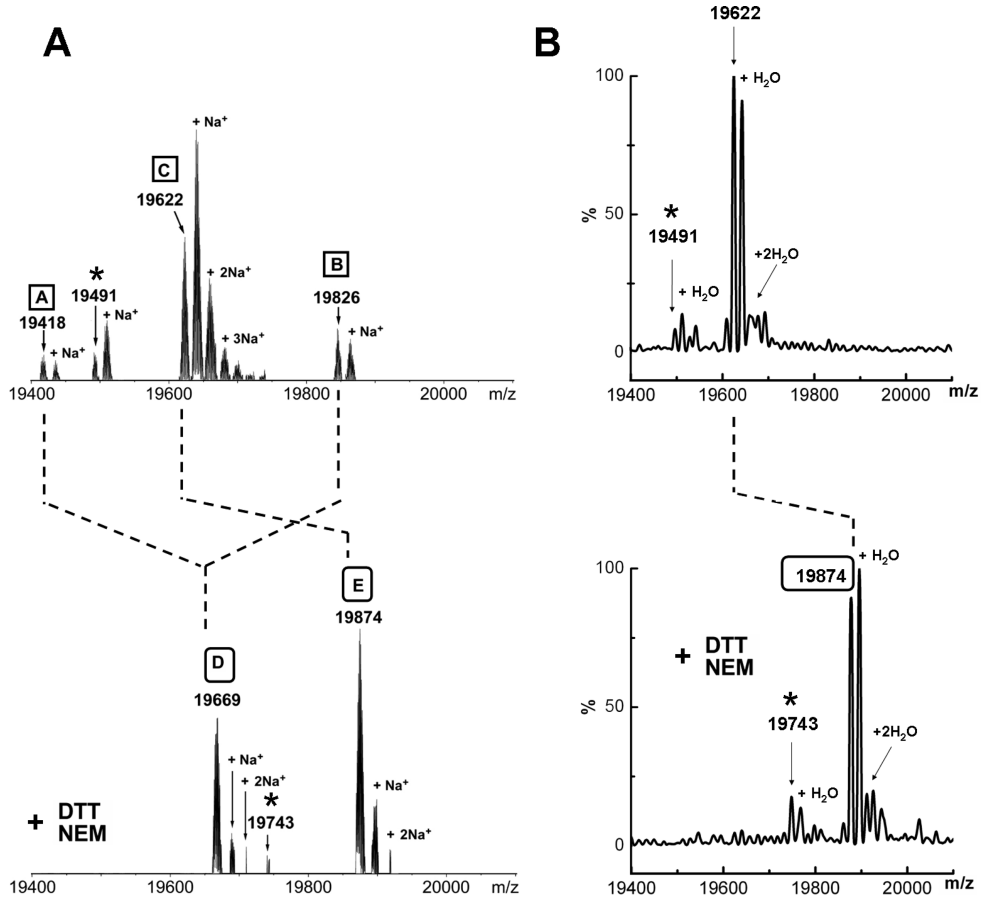

FIGURE 3: ESI mass spectra of the products of the reaction of ***m*-P** with **1** (top) and the corresponding mass spectra following subsequent addition of DTT and NEM (bottom). (A) Reaction of ***m*-P** with **1** carried out under unfolding conditions (see Scheme 2 for structures A−E). (B) Reaction of ***m*-P** with **1** carried out under folding conditions (Scheme 3). The major peaks at *m*/*z* 19622 and 19784 are due to ***fm*-P_{ox}** and the NEM derivative, E, respectively. The asterisks indicate the corresponding peaks for the impurity resulting from N-terminal methionine truncation. Dotted lines indicate how the peaks are related in the DTT/NEM reaction.

The mass spectra indicate that ***fm*-P_{ox}** is formed directly in one step from the reaction of ***m*-P** and **1** under unfolding conditions. Although this is the major product, there is a significant amount of the byproducts, and so a different approach was developed to suppress the intramolecular reactions shown in Scheme 2. Since the cysteines were specifically placed at sites on the surface of the folded protein that are too far apart to be bridged by **1**, the unwanted intramolecular side reactions that arise from the higher effective molarity in the unfolded state should be severely disfavored in the folded protein (*24, 58*). Thus, the reaction was carried out starting from ***m*-P** in the folded state, as shown in Scheme 3. The level of acetonitrile required to dissolve **1** at high concentrations does not perturb the folded state significantly, as confirmed by the CD and ^{1}H NMR spectra of ***wt*-P** in 30% (v/v) acetonitrile. After functionalization with **1**, subsequent reaction steps were identical to the ones described for the preparation of ***fwt*-P** and were carried out under unfolding conditions through the addition of 2 M GuHCl (Schemes 1 and 3). Under these conditions, intramolecular oxidation of the two aromatic thiols is favored over intermolecular oxidation because of the relatively high effective molarity in the unfolded state (*24, 58*). The final product (***fm*-P_{ox}**) was obtained with no significant byproducts, as shown by the mass spectrum (Figure 3B). The identity of ***fm*-P_{ox}** was confirmed using the DTT/NEM labeling experiment, as described above (Scheme 3 and Figure 3B).

^{1}H NMR Spectroscopy. To determine the effects of cross-linking residues 108 and 118 on the overall conformational properties of N-PGK, ^{1}H NMR spectra of ***fm*-P_{ox}** were recorded and compared with those of ***m*-P** and ***wt*-P** (Figure 4). The spectra of ***m*-P** and ***wt*-P** are similar and show the chemical shift dispersion typical of native proteins, whereas the spectrum of ***fm*-P_{ox}** is quite different. In particular, the degree of resonance dispersion is greatly reduced in the spectrum of ***fm*-P_{ox}**: for example, there are no signals in the high field region (from 0.5 to −2.0 ppm). Such changes are indicative of a change in conformation to a considerably less ordered structure. Upon addition of DTT, which cleaves the aromatic disulfide cross-link, resonances appear between 0.5 and −2.0 ppm, indicating that the reduced protein ***fm*-P_{red}** adopts a nativelike conformation and that it is the geometrical constraints rather than the chemical properties of the cross-link that perturb the structure. The nativelike behavior of ***fm*-P_{red}** (and of ***m*-P**) was maintained after addition of 1.0 M GuHCl (Figure 1 of the Supporting Information), indicating that the fold stability is not greatly compromised by the presence of the residual components of the reduced (cleaved) cross-linker. Hence, the NMR data indicate that the aromatic disulfide cross-link between residues 108 and 118 constrains ***fm*-P_{ox}** in a non-native state with no well-defined tertiary structure and that this constraint can be released by chemical cleavage to regenerate folded protein.

Scheme 3: Procedure Used for the Preparation of the Cross-Linked ***fm*-$\mathbf{P_{ox}}$** Using Native Conditions for the First Step of the Reaction (i) and Unfolding Conditions for Subsequent Steps[a]

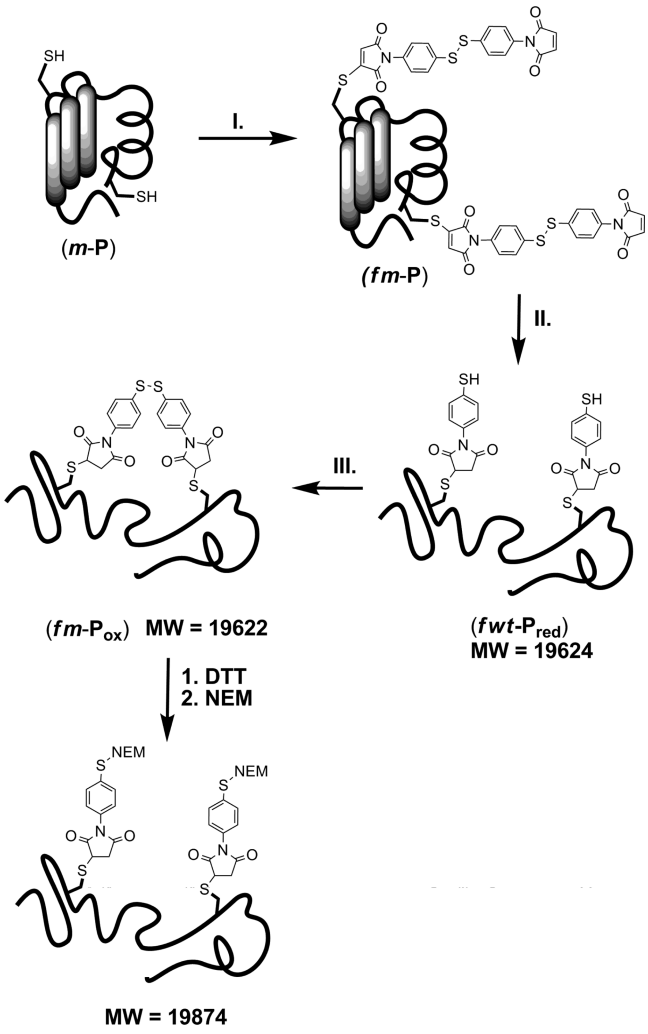

[a] Conditions: (i) 100 μM **1**, 50 mM sodium phosphate (pH 6.5), 3 mM NaN_3, 30% CH_3CN; (ii) 50 mM sodium phosphate (pH 7.0), 3 mM NaN_3, 1 mM DTT, 3 M GuHCl; (iii) 50 mM sodium phosphate (pH 7.0), 3 mM NaN_3, 100 mM NaCl. The structure of the product obtained after sequential addition of DTT and NEM to ***fm*-$\mathbf{P_{ox}}$** is identical to product E in Scheme 2.

Circular Dichroism Spectroscopy. To assess the effects of cross-linking residues 108 and 118 on the secondary structure of N-PGK, far-UV CD spectra of ***fm*-$\mathbf{P_{ox}}$** were recorded and compared with those of ***m*-P** and ***fm*-$\mathbf{P_{red}}$** (Figure 5A). The CD spectrum of ***fm*-$\mathbf{P_{ox}}$** under native conditions shows substantial secondary structure content, although the shape of the spectrum is distinguishable from those of ***m*-P** and ***fm*-$\mathbf{P_{red}}$**, which overlay closely (Figure 5A). The spectra of ***m*-P** and ***fm*-$\mathbf{P_{red}}$** also overlay closely with that of ***wt*-P** (Figure 3 of the Supporting Information). The differences in the spectrum of ***fm*-$\mathbf{P_{ox}}$** are well-represented by the relative molar ellipticities at 208 and 222 nm (characteristic of the contribution from α-helical conformations). In the cases of ***m*-P** and ***fm*-$\mathbf{P_{red}}$**, the ellipticity at 222 nm is higher than the ellipticity at 208 nm, while for ***fm*-$\mathbf{P_{ox}}$**, the opposite is observed. This is consistent with some disruption of helix length in ***fm*-$\mathbf{P_{ox}}$**. In addition, the CD spectrum of ***fm*-$\mathbf{P_{ox}}$** shows a weak band at 240−280 nm,

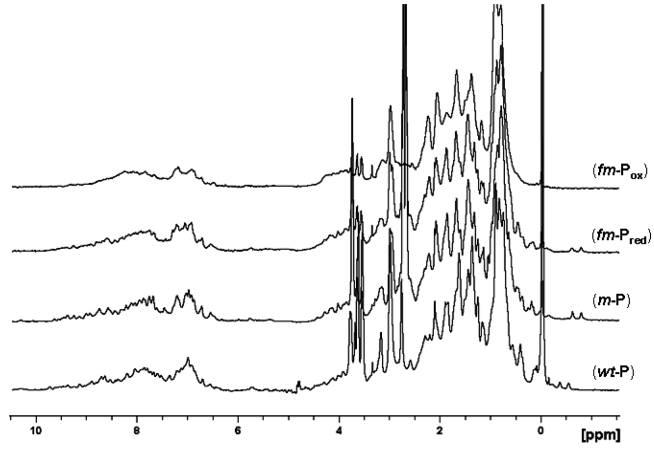

FIGURE 4: ^{1}H NMR spectra (600 MHz) of ***wt*-P** (100 μM), ***m*-P** (100 μM), ***fm*-$\mathbf{P_{ox}}$** (80 μM), and ***fm*-$\mathbf{P_{red}}$** (80 μM). Samples were prepared in 50 mM sodium phosphate (pH 7.0), 100 mM NaCl, 3 mM NaN_3, and 10% D_2O and contained 1 mM DTT for ***m*-P** and ***fm*-$\mathbf{P_{red}}$**. All samples contained TSP as an internal reference.

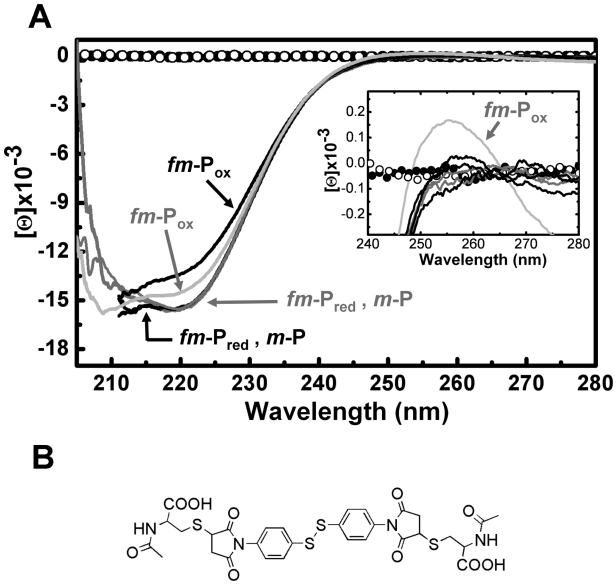

FIGURE 5: Far-UV CD spectra of ***fm*-$\mathbf{P_{ox}}$**, ***fm*-$\mathbf{P_{red}}$**, and ***m*-P**, with an expansion of the region between 240 and 280 nm (inset). (A) Spectra recorded under native conditions (gray lines) and in the presence of 2 M urea (black lines), the latter shown only at wavelengths longer than 210 nm because of the high absorbance of the denaturant below 210 nm. Empty and filled circles represent the far-UV CD of the model disulfide control compound shown in panel B, in the absence of denaturant, before and after addition of DTT, respectively. Identical spectra were obtained for the model compound in the presence of the same concentration of denaturant used for the proteins (data not shown). (B) Structure of the model disulfide used as a control for the CD measurements and for the determination of the concentration of ***fm*-$\mathbf{P_{ox}}$** (see Figure 2 of the Supporting Information). Spectra were recorded with 20 μM disulfide or protein in 50 mM sodium phosphate, 100 mM NaCl, and 3 mM NaN_3 (pH 7.0). DTT (1 mM) was added to the species containing thiols.

which is absent in ***m*-P** and ***wt*-P** (Figure 5A, inset, and Figure 3 of the Supporting Information). This band is a feature of the aromatic disulfide bond in the context of the protein and is abolished upon addition of DTT to ***fm*-$\mathbf{P_{ox}}$**. The contributions of the aromatic disulfide and thiols to the far-UV CD spectra of the functionalized proteins are negligibly small, as illustrated by the observation that there is no contribution at 208 or 222 nm in the CD spectrum of

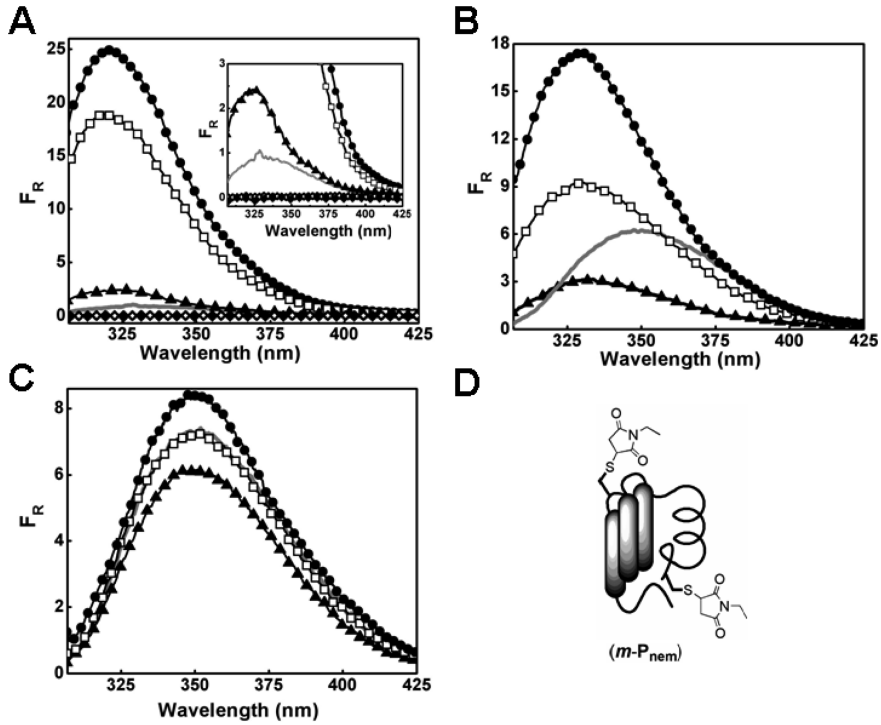

FIGURE 6: Relative fluorescence emission (F_R) spectra of ***m*-P** (□), ***m*-P_{nem}** (●), ***fm*-P_{ox}** (gray line), and ***fm*-P_{red}** (▲). (A) Spectra recorded under native conditions. Empty and filled diamonds represent the spectra of the model disulfide shown in Figure 5 before and after addition of DTT, respectively. The inset shows an expansion of the spectrum in the emission region of ***fm*-P_{ox}**, ***fm*-P_{red}**, and the model disulfide (symbols as in the main panel). (B) Spectra of the proteins recorded in the presence of intermediate levels of chemical denaturant (1.4 M GuHCl). (C) Spectra of the proteins recorded under unfolding conditions (2.0 M GuHCl). (D) Schematic representation of ***m*-P_{nem}**. For all the measurements, samples were prepared with proteins or the model disulfide (2 μM) in 50 mM sodium phosphate, 3 mM NaN_3, and 100 mM NaCl (pH 7.0). For ***m*-P**, ***fm*-P_{red}**, and the reduced model disulfide, 1 mM DTT was also present.

a model disulfide composed of two *N*-acetylcysteine derivatives attached to **1**, with and without DTT (Figure 5).

The data show that when the cross-link is in place between residues 108 and 118, a substantial degree of secondary structure can still form in ***fm*-P_{ox}**. One consequence of this is that, under fully native conditions, the overall amplitude changes in the CD responses that report on the refolding trajectory are small (though individual components of the refolding trajectory may, of course, still have large amplitudes). However, since the presence of the cross-link has an overall destabilizing effect on the protein fold (Figure 4 and data presented below), the addition of relatively low concentrations of chemical denaturant should increase the differences in the CD responses of ***fm*-P_{ox}** and ***fm*-P_{red}**. This strategy was adopted in early investigations of the use of phototriggering to observe fast events in protein folding (*59, 60*). Although guanidine hydrochloride was used in the preparation of ***fm*-P_{ox}**, urea was used as the denaturant to test this hypothesis, as the UV absorption of the chloride ions compromises the signal-to-noise ratio of far-UV CD spectra. While this has limited consequences for equilibrium measurements, the absorption properties of chloride ions can have substantial effects on the quality of kinetic refolding transients that can be measured using CD. The CD measurements in the presence of urea are shown in Figure 5.

In the presence of 2 M urea, the CD spectrum of ***fm*-P_{ox}** shows a decrease (20%) in the intensity at 222 nm compared to ***m*-P** and ***wt*-P** (Figure 5A and Figure 3 of the Supporting Information) markedly larger than that observed in the absence of denaturant. Upon addition of DTT, the resulting spectrum of ***fm*-P_{red}** is again similar to those of ***m*-P** and ***wt*-P**. In addition, the band at 240 nm observed for ***fm*-P_{ox}**, which is 10-fold weaker in the presence of urea, is abolished by addition of DTT (Figure 5A, inset). This confirms that the addition of denaturant more strongly perturbs the secondary structure of the cross-linked ***fm*-P_{ox}** compared with ***wt*-P**, ***m*-P**, and ***fm*-P_{red}**. Hence, the amplitude of the overall changes in CD response when refolding is triggered can be modulated using low concentrations of chemical denaturants. Overall, the behaviors of the CD data and the ^{1}H NMR measurements are consistent with ***fm*-P_{ox}** being a partially unfolded, molten globule state (*14*−*18*), when the cross-link is between residues 108 and 118.

Fluorescence Spectroscopy. Fluorescence spectra were recorded for ***fm*-P_{ox}**, ***fm*-P_{red}**, ***m*-P**, the model small molecule disulfide, and an additional control protein (***m*-P_{nem}**) (Figure 6). ***wt*-P** was not used in these measurements, as it has no tryptophan residue. There are potential complications with ***m*-P**, because DTT is required to maintain the thiols in the reduced state, and DTT can quench tryptophan fluorescence to some extent. Therefore, the exposed thiols of ***m*-P** were functionalized with NEM to give ***m*-P_{nem}**, which is a more reliable control with increased fluorescence (because of the lack of requirement for DTT in the solution), but properties otherwise similar to those of ***m*-P** (Figure 6). Under native conditions, the fluorescence intensity of ***fm*-P_{ox}** is nearly 20-fold less than the intensity of ***m*-P_{nem}**. Upon addition of DTT, a recovery of 2.5-fold in the intensity is observed for ***fm*-P_{red}** compared with that for ***fm*-P_{ox}** (inset of Figure 6A). There is no detectable fluorescence for the model aromatic

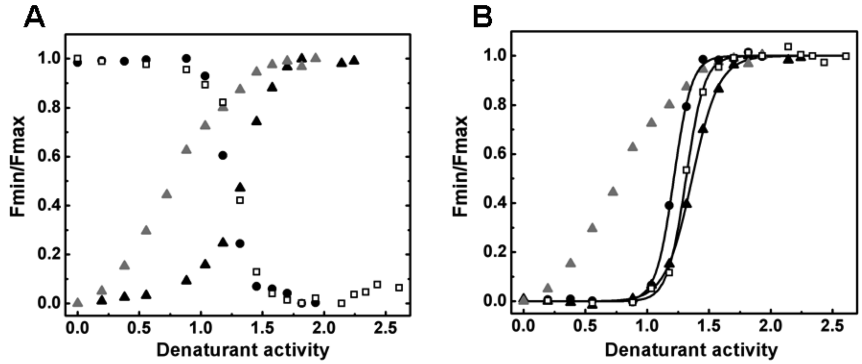

FIGURE 7: Equilibrium unfolding profiles of ***m*-P** (□), ***m*-P_{nem}** (●), ***fm*-P_{ox}** (gray triangles), and ***fm*-P_{red}** (▲), obtained by following the tryptophan emission at increasing concentrations of GuHCl. (A) Data are normalized relative to the observed fluorescence of the unfolded protein. (B) Data are normalized relative to the fraction of the unfolded protein, and the lines represent the fitting of the changes in fluorescence to a two-state model for ***m*-P**, ***m*-P_{nem}**, and ***fm*-P_{red}**. For the normalization of data for ***fm*-P_{ox}**, the emission observed under native conditions was taken as the zero fraction unfolded.

disulfide or the reduced thiol (Figure 6A and Figure 4 of the Supporting Information), and so the fluorescence observed for the cross-linked protein is due exclusively to the tryptophan.

The quenching in the fluorescence of ***fm*-P_{red}** relative to that of ***m*-P_{nem}** raises the possibility that ***fm*-P_{ox}** does not fully revert to a native state upon addition of DTT, but this is inconsistent with the exclusively nativelike NMR properties of ***fm*-P_{red}** (Figure 4). A more likely explanation for the reduced fluorescence emission of ***fm*-P_{red}** relative to those of ***m*-P** and ***m*-P_{nem}** is a coupling between the tryptophan and the chromophore of the cross-linker, leading to fluorescence quenching. A similar effect would account for the reduced fluorescence emission of ***fm*-P_{ox}**. The increase in the fluorescence emission of ***fm*-P_{red}** relative to that of ***fm*-P_{ox}** under native conditions (Figure 6A) is consistent with the aromatic disulfide being a stronger quencher of tryptophan than the aromatic thiols, and this trend is also observed in many proteins upon reduction of disulfides that are located in the vicinity of tryptophan residues (i.e., cystine is normally a more powerful quencher of tryptophan fluorescence than cysteine) (*61*).

Fluorescence quenching resulting from the aromatic cross-link also accounts for the denaturant dependence of the fluorescence intensity observed for ***fm*-P_{ox}** and ***fm*-P_{red}** relative to ***m*-P_{nem}** and ***m*-P**. On denaturation with 2.0 M GuHCl, the fluorescence of ***fm*-P_{ox}** and ***fm*-P_{red}** increases, whereas the fluorescence of ***m*-P** and ***m*-P_{nem}** decreases (Figure 6A,C). For ***m*-P** and ***m*-P_{nem}**, unfolding leads to a decrease in the intensity of the fluorescence because the tryptophan becomes exposed to the solvent. For ***fm*-P_{ox}** and ***fm*-P_{red}**, unfolding leads to an increase in the average separation of the tryptophan and the aromatic disulfide/aromatic thiols, weakening the interaction between the chromophores that are responsible for fluorescence quenching. This leads to two effects. First, at an intermediate concentration of denaturant (Figure 6B), the intensity of ***fm*-P_{ox}** is higher than that of ***fm*-P_{red}**, contrary to what is observed under native conditions. Second, in high concentrations of denaturant, the fluorescence spectra are similar for all four proteins (Figure 6C) because the quenching due to the aromatic disulfide or aromatic thiols is largely abolished and the predominant quenching effect is the result of the exposure of tryptophan to the solvent.

Table 1: Summary of the Folding Parameters for ***m*-P**, ***fm*-P_{red}**, and ***m*-P_{nem}**[a]

protein	ΔG (kcal/mol)	m_D (M^{-1})	$D_{0.5}$ (M)
***m*-P**	-8.6 ± 0.6	-13.4 ± 0.6	1.3
***fm*-P_{red}**	-8.3 ± 0.4	-9.1 ± 0.5	1.3
***m*-P_{nem}**	-5.9 ± 0.2	-13.8 ± 0.7	1.2

[a] The values are reported as a function of denaturant activity (D) (*47*). The value of denaturant activity corresponding to the midpoint of the unfolding transition is reported ($D_{0.5}$).

Importantly, the wavelength of the fluorescence emission maximum observed for ***fm*-P_{ox}** is red-shifted relative to those of the other three proteins, indicating that the tryptophan is in a different environment in the cross-linked protein compared with the natively folded species. This effect is particularly apparent at intermediate denaturant concentrations [1.4 M GuHCl (Figure 6B)], where the fluorescence emission maximum of ***fm*-P_{ox}** is in the range of unfolded proteins. The blue shift of the fluorescence emission maximum of ***fm*-P_{red}** relative to that of ***fm*-P_{ox}** indicates the recovery of the fluorescence properties of ***fm*-P_{ox}** toward a more nativelike environment for the tryptophan upon cleavage of the aromatic disulfide cross-link. Thus, the tryptophan could be used as a time-dependent spectroscopic probe for refolding of ***fm*-P_{ox}** upon cleavage of the aromatic disulfide.

Equilibrium Unfolding Experiments. Fluorescence spectroscopy was used to quantify the effects of denaturant on the folding properties of proteins ***m*-P**, ***m*-P_{nem}**, ***fm*-P_{red}**, and ***fm*-P_{ox}**, and the equilibrium unfolding measurements are shown in Figure 7. Reversibility throughout the folding transitions of all four proteins was established by comparing fluorescence emission spectra on concentration and on dilution of the denaturant over the entire concentration range. For ***m*-P**, ***m*-P_{nem}**, and ***fm*-P_{red}**, the experimental data fitted well to a two-state model (*47*), where only the unfolded and folded states are significantly populated at equilibrium, and the resulting thermodynamic parameters are listed in Table 1. These three proteins show very similar transition midpoints, despite the differences in the fluorescence properties of their folded states (Figure 6A). In contrast, the cross-linked protein ***fm*-P_{ox}** shows clearly different behavior, though the lack of a pretransition baseline in the unfolding of ***fm*-P_{ox}** and the potential failure of a two-state model to describe the transition adequately (*14*−*18*) prevent any quantitative determination of the fold stability of the cross-linked protein.

Qualitatively, the data indicate that ***fm*-$\mathbf{P_{ox}}$** is strongly destabilized compared to the other proteins, which is consistent with the CD observations that there are larger perturbations of structure for the cross-linked protein on addition of denaturant compared with ***fm*-$\mathbf{P_{red}}$** and ***m*-P** (Figure 5A). At GuHCl concentrations of 0.5−1.3 M (corresponding to 0.46−1.1 M on the activity scale in Figure 7), the folded state is predominant for ***m*-P**, ***m*-$\mathbf{P_{nem}}$**, and ***fm*-$\mathbf{P_{red}}$**, while the cross-linked protein (***fm*-$\mathbf{P_{ox}}$**) populates more unfolded species to a substantial extent. Like the CD observations described above, this indicates that time-resolved measurements after cleavage of the aromatic cross-link would have larger overall amplitudes in the presence of low concentrations of denaturant.

The thermodynamic parameters determined for ***m*-P** and ***m*-$\mathbf{P_{nem}}$** (Table 1) are very similar to published data for ***wt*-P** and single-cysteine variants of ***wt*-P** (*44, 47, 57*). This indicates that neither the four mutations in ***m*-P** nor functionalization of the exposed surface thiols perturbs the stability of the folded protein significantly. In the case of ***fm*-$\mathbf{P_{red}}$**, the thermodynamic stability and *m* values observed are somewhat lower than the values found for ***m*-P** and ***m*-$\mathbf{P_{nem}}$**. Changes in *m* values are proportional to the surface area exposed as a result of the unfolding transition and are affected by the amount of residual structure in the denatured state (*13*). The latter argument has been used as an explanation for large changes in *m* values observed in the unfolding transition of the single-cysteine mutant of ***wt*-P** (*44*). In the case of ***fm*-$\mathbf{P_{red}}$**, the presence of the two aromatic thiols can affect both the hydrophobic area exposed during unfolding and the structure of the denaturated state and, most likely, contributes to its relatively low unfolding *m* value compared with those of ***m*-P** and ***m*-$\mathbf{P_{nem}}$** (*13*). The ^{1}H NMR, CD, and fluorescence spectra of ***fm*-$\mathbf{P_{red}}$** suggest that the low *m* values are not due to significant perturbation of the native state (Figures 4, 5A, and 6A).

CONCLUSIONS

We have developed a general method for functionalizing proteins with a cleavable cross-linker and demonstrated its viability using the 174-residue protein N-PGK. The cross-linker is readily attached to cysteine residues introduced at the desired point of cross-linking, and the protocol appears sufficiently robust in terms of yield of cyclized protein (40% of the original protein in the case studied here). The method affords a cyclic polypeptide that is readily probed in terms of the disruption of the native fold, and cleavage of the cross-linker leads to the quantitative re-establishment of a normally folded protein.

In our test protein, where residues 108 and 118 of N-PGK are cross-linked, it was shown using NMR spectroscopy that under normal solution conditions the tertiary structure of the cross-linked protein is largely perturbed, while CD measurements indicate that the protein retains a substantial degree of secondary structure, albeit it is somewhat different in nature from the native protein. Fluorescence measurements show that the single tryptophan residue is in a hydrophobic environment, and together, these observations point to this cross-linked protein behaving as a typical molten globule state. The denaturant concentration dependence of the fluorescence spectra further supports this conclusion, showing the decline in the cooperativity of the unfolding transition that is characteristic of molten globule states (*14*−*18*). The ability of cross-linked N-PGK to populate a relatively stable molten globule state at low denaturant concentrations is consistent with previous predictions for wild-type N-PGK from the denaturant dependence of its NMR spectra (*62*).

The contrasting denaturant concentration dependences of the cross-linked protein and the cross-link cleaved protein allow the exploration of the folding landscape to be expanded; for example, in our test protein, folding can be initiated from an ensemble dominated by molten globule species, or in the presence of small concentrations of denaturant, it is possible to find conditions under which the cross-linked ensemble is predominantly unfolded, while the cleaved form remains predominantly folded. This sort of behavior will not necessarily be encountered in all possible cross-linking positions of N-PGK (nor, indeed, with other proteins), where more unfolded or more folded species may dominate the ensemble populated by the cross-linked protein, even in the absence of denaturant. Importantly, the methodology described here allows a wide range of these possibilities to be readily tested, so that a fuller picture of the free energy landscape for folding can be developed. Once the cross-link is broken, each starting distribution of conformers is subject to the free energy landscape of a protein that folds to a native structure and its progress toward the native state will report on that landscape. In addition to the use of the methodology in the triggering of protein folding, there is also wide potential use for the activation of proteins in a rapid and coherent manner, at a rate set by the transition from the conformational ensemble selected by the cross-linker to the native fold.

ACKNOWLEDGMENT

We thank Svetlana Sedelnikova and Tooba Alizadeh (The University of Sheffield) for assistance in protein expression and purification, Simon Thorpe (The University of Sheffield) and Liam McDonnell (University of Warwick, Warwick, U.K.) for assistance in the mass spectrometry analysis, and Salvador Tomas for critical reading of the manuscript.

SUPPORTING INFORMATION AVAILABLE

^{1}H NMR and CD spectra of the cross-linked and native proteins in the presence of denaturant, UV−vis absorption spectra of cross-linked, native proteins, and model disulfide and fluorescence emission spectra recorded in the control experiments. This material is available free of charge via the Internet at http://pubs.acs.org.

REFERENCES

1. Anfinsen, C. B. (1973) Principles that govern folding of protein chains. *Science 181*, 223–230.
2. Shakhnovich, E. (2006) Protein folding thermodynamics and dynamics: Where physics, chemistry, and biology meet. *Chem. Rev. 106*, 1559–1588.
3. Oliveberg, M., and Wolynes, P. G. (2005) The experimental survey of protein-folding energy landscapes. *Q. Rev. Biophys. 38*, 245–288.
4. Daggett, V., and Fersht, A. (2003) The present view of the mechanism of protein folding. *Nat. Rev. Mol. Cell Biol. 4*, 497–502.
5. Baker, D. (2000) A surprising simplicity to protein folding. *Nature 405*, 39–42.

6. Tulla-Puche, J., Getun, I. V., Woodward, C., and Barany, G. (2004) Native-like conformations are sampled by partially folded and disordered variants of bovine pancreatic trypsin inhibitor. *Biochemistry 43*, 1591–1598.
7. Jaenicke, R. (1999) Stability and folding of domain proteins. *Prog. Biophys. Mol. Biol. 71*, 155–241.
8. Darby, N. J., Morin, P. E., Talbo, G., and Creighton, T. E. (1995) Refolding of bovine pancreatic trypsin-inhibitor via non-native disulfide intermediates. *J. Mol. Biol. 249*, 463–477.
9. Ptitsyn, O. B. (1987) Protein folding: Hypotheses and experiments. *J. Protein Chem. 6*, 273–293.
10. Chiti, F., and Dobson, C. M. (2006) Protein misfolding, functional amyloid, and human disease. *Annu. Rev. Biochem. 75*, 333–366.
11. Jackson, G. S., Hosszu, L. L. P., Power, A., Hill, A. F., Kenney, J., Saibil, H., Craven, C. J., Waltho, J. P., Clarke, A. R., and Collinge, J. (1999) Reversible conversion of monomeric human prion protein between native and fibrilogenic conformations. *Science 283*, 1935–1937.
12. Prusiner, S. B. (1998) Prions. *Proc. Natl. Acad. Sci. U.S.A. 95*, 13363–13383.
13. Dill, K. A., and Shortle, D. (1991) Denatured states of proteins. *Annu. Rev. Biochem. 60*, 795–825.
14. Nishimura, C., Dyson, H. J., and Wright, P. E. (2008) The kinetic and equilibrium molten globule intermediates of apoleghemoglobin differ in structure. *J. Mol. Biol. 378*, 715–725.
15. Staniforth, R. A., Giannini, S., Higgins, L. D., Conroy, M. J., Hounslow, A. M., Jerala, R., Craven, C. J., and Waltho, J. P. (2001) Three-dimensional domain swapping in the folded and molten-globule states of cystatins, an amyloid-forming structural superfamily. *EMBO J. 20*, 4774–4781.
16. Fink, A. L. (1995) Compact intermediate states in protein-folding. *Annu. Rev. Biophys. Biomol. Struct. 24*, 495–522.
17. Ptitsyn, O. B. (1995) Molten globule and protein folding. *Adv. Protein Chem. 47*, 83–229.
18. Kuwajima, K. (1989) The molten globule state as a clue for understanding the folding and cooperativity of globular-protein structure. *Proteins: Struct., Funct., Genet. 6*, 87–103.
19. Smith, D. P., Jones, S., Serpell, L. C., Sunde, M., and Radford, S. E. (2003) A systematic investigation into the effect of protein destabilisation on β2-microglobulin amyloid formation. *J. Mol. Biol. 330*, 943–954.
20. Mayor, U., Grossmann, J. G., Foster, N. W., Freund, S. M. V., and Fersht, A. R. (2003) The denatured state of engrailed homeodomain under denaturing and native conditions. *J. Mol. Biol. 333*, 977–991.
21. Kouvatsos, N., Meldrum, J. K., Searle, M. S., and Thomas, N. R. (2006) Coupling ligand recognition to protein folding in an engineered variant of rabbit ileal lipid binding protein. *Chem. Commun.,* 4623–4625.
22. Kohn, J. E., and Plaxco, K. W. (2005) Engineering a signal transduction mechanism for protein-based biosensors. *Proc. Natl. Acad. Sci. U.S.A. 102*, 10841–10845.
23. Creighton, T. E. (1974) Intermediates in refolding of reduced pancreatic trypsin-inhibitor. *J. Mol. Biol. 87*, 579.
24. Creighton, T. E. (1975) Interactions between cysteine residues as probes of protein conformation: Disulfide bond between cys-14 and cys-38 of pancreatic trypsin-inhibitor. *J. Mol. Biol. 96*, 767–776.
25. Kolano, C., Helbing, J., Kozinski, M., Sander, W., and Hamm, P. (2006) Watching hydrogen-bond dynamics in a β-turn by transient two-dimensional infrared spectroscopy. *Nature 444*, 469–472.
26. Lu, H. S. M., Volk, M., Kholodenko, Y., Gooding, E., Hochstrasser, R. M., and DeGrado, W. F. (1997) Aminothiotyrosine disulfide, an optical trigger for initiation of protein folding. *J. Am. Chem. Soc. 119*, 7173–7180.
27. Ghosh, K., Ozkan, S. B., and Dill, K. A. (2007) The ultimate speed limit to protein folding is conformational searching. *J. Am. Chem. Soc. 129*, 11920–11927.
28. Roder, H., Maki, K., and Cheng, H. (2006) Early events in protein folding explored by rapid mixing methods. *Chem. Rev. 106*, 1836–1861.
29. Myers, J. K., and Oas, T. G. (2002) Mechanisms of fast protein folding. *Annu. Rev. Biochem. 71*, 783–815.
30. Eaton, W. A., Munoz, V., Hagen, S. J., Jas, G. S., Lapidus, L. J., Henry, E. R., and Hofrichter, J. (2000) Fast kinetics and mechanisms in protein folding. *Annu. Rev. Biophys. Biomol. Struct. 29*, 327–359.
31. Mayor, U., Johnson, C. M., Daggett, V., and Fersht, A. R. (2000) Protein folding and unfolding in microseconds to nanoseconds by experiment and simulation. *Proc. Natl. Acad. Sci. U.S.A. 97*, 13518–13522.
32. Chen, R. P. Y., Huang, J. J. T., Chen, H. L., Jan, H., Velusamy, M., Lee, C. T., Fann, W. S., Larsen, R. W., and Chan, S. I. (2004) Measuring the refolding of β-sheets with different turn sequences on a nanosecond time scale. *Proc. Natl. Acad. Sci. U.S.A. 101*, 7305–7310.
33. Huang, C. Y., He, S., DeGrado, W. F., McCafferty, D. G., and Gai, F. (2002) Light-induced helix formation. *J. Am. Chem. Soc. 124*, 12674–12675.
34. Kumita, J. R., Smart, O. S., and Woolley, G. A. (2000) Photocontrol of helix content in a short peptide. *Proc. Natl. Acad. Sci. U.S.A. 97*, 3803–3808.
35. Zhu, Y.; Wang, T., and Gai, F. (2005) Laser-induced *T*-jump method: A non-conventional photoreleasing approach to study protein folding. In *Dynamic Studies in Biology* (Goeldner, M., and Givens, R., Eds.) 1st ed., pp 461−479, Wiley-VCH, Weinheim, Germany.
36. Hodgson, D. R. W., and Sanderson, J. M. (2004) The synthesis of peptides and proteins containing non-natural amino acids. *Chem. Soc. Rev. 33*, 422–430.
37. Volk, M. (2001) Fast initiation of peptide and protein folding processes. *Eur. J. Org. Chem. 14*, 2605–2621.
38. Shandiz, A. T., Capraro, B. R., and Sosnick, T. R. (2007) Intramolecular cross-linking evaluated as a structural probe of the protein folding transition state. *Biochemistry 46*, 13711–13719.
39. Weikl, T. R., and Dill, K. A. (2003) Folding kinetics of two-state proteins: Effect of circularization, permutation, and crosslinks. *J. Mol. Biol. 332*, 953–963.
40. Milanesi, L., Reid, G. D., Beddard, G. S., Hunter, C. A., and Waltho, J. P. (2004) Synthesis and photochemistry of a new class of photocleavable protein cross-linking reagents. *Chem.−Eur. J. 10*, 1705–1710.
41. Palmblad, M., Hakansson, K., Hakansson, P., Feng, X. D., Cooper, H. J., Giannakopulos, A. E., Green, P. S., and Derrick, P. J. (2000) A 9.4 T Fourier transform ion cyclotron resonance mass spectrometer: Description and performance. *Eur. J. Mass Spectrom. 6*, 267–275.
42. Mohamadi, F., Richards, N. G. J., Guida, W. C., Liskamp, R., Lipton, M., Caufield, C., Chang, G., Hendrickson, T., and Still, W. C. (1990) Macromodel: An integrated software system for modeling organic and bioorganic molecules using molecular mechanics. *J. Comput. Chem. 11*, 440–467.
43. Davies, G. J., Gamblin, S. J., Littlechild, J. A., Dauter, Z., Wilson, K. S., and Watson, H. C. (1994) Structure of the Adp complex of the 3-phosphoglycerate kinase from *Bacillus stearothermophilus* at 1.65 angstrom. *Acta Crystallogr. D50*, 202–209.
44. Cliff, M. J., Alizadeh, T., Jelinska, C., Craven, C. J., Staniforth, R. A., and Waltho, J. P. (2006) A thiol labelling competition experiment as a probe for sidechain packing in the kinetic folding intermediate of N-PGK. *J. Mol. Biol. 364*, 810–823.
45. Ellman, G. L. (1959) Tissue sulfhydryl groups. *Arch. Biochem. Biophys. 82*, 70–77.
46. Creighton, T. E. (1984) Disulfide bond formation in proteins. *Methods Enzymol. 107*, 305–329.
47. Parker, M. J., Spencer, J., and Clarke, A. R. (1995) An integrated kinetic-analysis of intermediates and transition-states in protein-folding reactions. *J. Mol. Biol. 253*, 771–786.
48. Santoro, M. M., and Bolen, D. W. (1988) Unfolding free-energy changes determined by the linear extrapolation method. 1. Unfolding of phenylmethanesulfonyl α-chymotrypsin using different denaturants. *Biochemistry 27*, 8063–8068.
49. Darby, N. J., Morin, P. E., Talbo, G., and Creighton, T. E. (1995) Refolding of bovine pancreatic trypsin-inhibitor via non-native disulfide intermediates. *J. Mol. Biol. 249*, 463–477.
50. Singh, R., and Kats, L. (1995) Catalysis of reduction of disulfide by selenol. *Anal. Biochem. 232*, 86–91.
51. Girouard, S., Houle, M. H., Grandbois, A., Keillor, J. W., and Michnick, S. W. (2005) Synthesis and characterization of dimaleimide fluorogens designed for specific labeling of proteins. *J. Am. Chem. Soc. 127*, 559–566.
52. Means, G. E., and Feeney, R. E. (1971) *Chemical Modifications of Proteins*, pp 110−114, Holden-Day, San Francisco.
53. Kolano, C., Helbing, J., Bucher, G., Sander, W., and Hamm, P. (2007) Intramolecular disulfide bridges as a phototrigger to monitor the dynamics of small cyclic peptides. *J. Phys. Chem. B 111*, 11297–11302.

54. Volk, M., Kholodenko, Y., Lu, H. S. M., Gooding, E. A., DeGrado, W. F., and Hochstrasser, R. M. (1997) Peptide conformational dynamics and vibrational stark effects following photoinitiated disulfide cleavage. *J. Phys. Chem. B 101*, 8607–8616.
55. Milanesi, L., Tomas, S., Hunter, C. A., Weinstein, J. A., Edge, R., Navaratnam, S., Waltho, J. P., and Best, J. (2008) A pulse radiolysis approach to fast reductive cleavage of a disulfide bond to uncage enzyme activity. *Free Radical Biol. Med. 45*, 1271–1278.
56. Hosszu, L. L. P., Craven, C. J., Spencer, J., Parker, M. J., Clarke, A. R., Kelly, M., and Waltho, J. P. (1997) Is the structure of the N-domain of phosphoglycerate kinase affected by isolation from the intact molecule? *Biochemistry 36*, 333–340.
57. Parker, M. J., Spencer, J., Jackson, G. S., Burston, S. G., Hosszu, L. L. P., Craven, C. J., Waltho, J. P., and Clarke, A. R. (1996) Domain behavior during the folding of a thermostable phosphoglycerate kinase. *Biochemistry 35*, 15740–15752.
58. Darby, N., and Creighton, T. E. (1995) Protein stability and folding: Theory and practice. In *Methods in Molecular Biology* (Shirley, B. A., Ed.) pp 219−252, Human Press Inc., Totowa, NJ.
59. Pascher, T., Chesick, J. P., Winkler, J. R., and Gray, H. B. (1996) Protein folding triggered by electron transfer. *Science 271*, 1558–1560.
60. Jones, C. M., Henry, E., Hu, Y., Cham, C.-K., Luck, S. D., Bhuyan, A., Roder, H., Hofrichter, J., and Eaton, W. A. (1993) Fast events in protein folding initiated by nanosecond laser photolysis. *Proc. Natl. Acad. Sci. U.S.A. 90*, 11860–11864.
61. Chakraborty, S., Ittah, V., Bai, P., Luo, L., Haas, E., and Peng, Z. Y. (2001) Structure and dynamics of the α-lactalbumin molten globule: Fluorescence studies using proteins containing a single tryptophan residue. *Biochemistry 40*, 7228–7238.
62. Reed, M. A. C., Jelinska, C., Syson, K., Cliff, M. J., Splevins, A., Alizadeh, T., Hounslow, A. M., Staniforth, R. A., Clarke, A. R., Craven, C. J., and Waltho, J. P. (2006) The Denatured State under Native Conditions: A Non-native-like Collapsed State of N-PGK. *J. Mol. Biol. 357*, 365–372.

BI801362F